

RiSi: Spectro-temporal RAN-agnostic Modulation Identification for OFDMA Signals

Daulet Kurmantayev, Dohyun Kwun, Hyoil Kim, *Senior Member, IEEE*, and Sung Whan Yoon *

Abstract—Blind modulation identification is essential for 6G’s RAN-agnostic communications, which identifies the modulation type of an incompatible wireless signal without any prior knowledge. Nowadays, research on blind modulation identification relies on deep convolutional networks that deal with a received signal’s raw I/Q samples, but they mostly are limited to single-carrier signal recognition thus not pragmatic for identifying spectro-temporal OFDM/OFDMA signals whose modulation varies with time and frequency. Therefore, this paper proposes RiSi, a semantic segmentation neural network designed to work on OFDMA’s spectrograms, by replacing vanilla DeepLabV3+’s 2D convolutions with ‘flattened’ convolutions to enforce the time-frequency orthogonality constraint and to achieve the grid-like pattern of OFDMA’s resource blocks, and by introducing three-channel inputs consisting of I/Q/amplitude. Then, we synthesized a realistic and effective dataset consisting of OFDMA signals with various channel impairments to train the proposed network. Moreover, we treated varying communication parameters as different domains to apply domain generalization methods, to enhance our model’s adaptability to diverse communication environments. Extensive evaluation shows that RiSi’s modulation identification accuracy reaches 86% averaged over four modulation types (BPSK, QPSK, 16-QAM, 64-QAM), while its domain generalization performance for unseen data has been also shown to be reliable.

Index Terms—6G, RAN-agnostic, modulation, OFDMA, semantic segmentation, domain generalization

I. INTRODUCTION

To pave the way toward 6G communications, there exist many technical proposals from the research community. Among them, a novel concept of RAN-agnostic communications is considered as one of 6G’s key enablers, which can promote more flexible utilization of time-frequency resources and better coexistence among heterogeneous radio access networks (RANs) [1], [2]. Unlike conventional radios that can only recognize compatible co-RAN devices, a RAN-agnostic node identifies the intrinsic features (e.g., modulation type) of the signals from coexisting incompatible devices even with no prior knowledge on their protocols nor frame structures.

*Daulet Kurmantayev, Dohyun Kwun, and Hyoil Kim are with the Department of Electrical Engineering, the Ulsan National Institute of Science and Technology (UNIST), Ulsan 44919, Korea (e-mail: {daulet,kwun1105,hkim}@unist.ac.kr). Sung Whan Yoon is with the Graduate School of AI, the Ulsan National Institute of Science and Technology (UNIST), Ulsan 44919, Korea (e-mail: shyoon8@unist.ac.kr). Hyoil Kim is the corresponding author.

The advent of RAN-agnostic communications will open a new way of coordinating the wireless devices belonging to heterogeneous RANs. Nowadays, the number of wireless devices and their diversity are ever-increasing, especially in the unlicensed bands due to the coexistence among WLAN, unlicensed-band cellular like 5G NR-U, IoT/LPWAN (Low Power Wide Area Network), etc. Such a tendency will further intensify with the recent release of additional 1.2GHz bandwidth in the U-NII bands at 6GHz. As a result, it is expected that in the beyond 5G era, highly-populated but incompatible devices will have to dynamically coordinate their coexistence while sharing spectrum resources.

Traditional inter-RAN coordination can be classified into explicit and implicit mechanisms. Explicit inter-RAN coordination requires developing a special protocol between incompatible RANs along with a dedicated control channel, thus not practical. On the other hand, implicit inter-RAN coordination relies on an open-loop control based on self-collectible information like SINR (Signal to Interference-and-Noise Ratio), which is simple to implement. Such an energy-detection-based approach, however, lacks to identify more sophisticated and complex inter-RAN relationships, possibly leading to a poor coexistence performance.

Unlike the aforementioned traditional approaches, RAN-agnostic communications leverage blind modulation identification to recognize the modulation type (and possibly other features) of an interference signal. Then, RAN-agnostic nodes can utilize thus-obtained knowledge for determining a more advantageous set of transmission parameters (e.g., modulation type, transmit power, phase shift in constellation) to better coexist with incompatible RANs/nodes, as will be shown in Section III with a motivating example. Furthermore, blind modulation identification requires much less time in rate adaptation than popular heuristic algorithms like Minstrel [3], since the former is realized at the PHY layer with a time scale of several to dozens of milliseconds while the latter is performed at the MAC layer in hundreds of milliseconds.

Although there recently have been many learning-based techniques introduced for blind modulation identification, most of them considered the classification of a signal modulated by a specific modulation class (e.g., m-PSK or m-QAM). There-

fore, such approaches are not instantly applicable to today’s most popular modulation schemes like OFDM and OFDMA, where a signal includes multiple modulation classes varying with spectro-temporal resource blocks/units. For instance, it is known that CNN-based approaches fail to discriminate between OFDM-BPSK and OFDM-QPSK signals, since an OFDM signal with a high number of subcarriers is approximated as a Gaussian process thus losing OFDM’s detailed features [4].

To tackle the resource-block-wise modulation diversity, this paper proposes applying semantic segmentation to the spectrogram of an OFDMA signal. Transforming the signal into a spectrogram is promising thanks to its natural ability to represent the signal’s spectrum varying with time and frequency. Then, semantic segmentation can detect the regions in the spectrogram corresponding to the resource blocks, so that their modulations can be determined individually.

This paper’s contributions are four-fold.

- First, we propose RiSi(RAN-agnostic identification of Signal interference), a communication-specific semantic segmentation neural network designed for blind modulation identification. The proposed network is evolved from vanilla DeepLab V3+ [5] by replacing its 2-dimensional convolutions with flattened convolution to better identify the grid-like pattern of varying modulations within OFDMA’s spectrogram, and by adding the third image channel representing the signal amplitude (along with two other channels for I and Q samples respectively).
- Second, we demonstrate an effective dataset construction strategy to maximize the identification accuracy, considering the characteristics of wireless signals, e.g., channel distortions and the difference in complexity levels among modulation types.
- Next, we evaluate and optimize the performance of RiSi while adjusting its architectural parameters. Our extensive experiments have shown that RiSi can achieve identification accuracy up to 92.9% for BPSK and up to 75.5% for QAMs, achieving 86% on average over BPSK, QPSK, 16-QAM, and 64-QAM. In addition, RiSi is shown to outperform other existing networks in the literature signifying the importance of adopting semantic segmentation.
- Finally, we apply state-of-the-art domain generalization methods (e.g., SWAD, MLDG) to our network to improve its performance in unseen scenarios to make it truly radio agnostic. Its generalization performance has been shown to improve in-domain by 4-5% and out-of-domain by 1-2% compared to a naive approach (i.e., ERM).

The paper is organized as follows. Section II overviews related work, and Section III presents a motivating example to show the benefit of RAN-agnostic communications for inter-RAN coexistence. Then, Section IV introduces the proposed architecture of RiSi, and Sections V and VI evaluate RiSi’s identification and domain generalization performances, respectively. Finally, the paper concludes with Section VII.

II. RELATED WORK

A. Neural Networks for modulation identification

Recently, there has been huge enhancement in the accuracy and computational complexity of the modulation classifiers, thanks to the adoption of deep learning techniques applied to raw I/Q samples. In this regard, various architectures have been proposed, including CNN, RNN, CRNN, LSTM, etc [6]–[9], all of which considered OFDM as a separate modulation class while ignoring its internal structure (i.e., varying modulations with resource blocks). When treating OFDM itself as a modulation class, however, [4] showed that OFDM signals experience the loss of internal features and become a white gaussian noise, thus not classifiable. Moreover, numerous CNN models proposed for signal constellation recognition require the modulation to remain constant for a long period of time to build a correct constellation, which is not possible for most communication systems.

As a remedy, this paper proposes using spectrogram since the nature of spectrogram allows for separation of a signal in the joint time-frequency domains. In fact, such spectrogram-based representation is more natural for the problem of OFDM modulation classification. Although there exist some studies on using spectrograms for modulation classification like [10]–[14], they considered to use spectrograms with CNN for only single-carrier signals, not utilizing the frequency resolution capability offered by the spectrograms.

B. Semantic segmentation for modulation recognition

[15] proposed the use of semantic segmentation networks on Choi-Williams spectrograms for modulation classification. They showed the ability of semantic segmentation to handle multiple signals spreading in the frequency domain. However, their work only used very simple and distinct modulations, as the research was done for radar systems rather than for the modulation families typically used in communication systems. Moreover, OFDM communication systems feature much more dense packing of subcarriers while some relationships between them are defined by a channel model, making it fundamentally different from simply having several uncorrelated signals in the same band.

In our work, we propose an evolved architecture of semantic segmentation, by replacing typically-used 2-dimensional convolutions in DeepLab V3+ [5] with flattened convolutions, to better address the spectro-temporal block-wise modulation populations in the OFDM spectrogram. Moreover, we further fine-tune various aspects of the spectrogram-based semantic segmentation architecture, in terms of realistic and effective dataset construction, hyper-parameter tuning, etc.

III. MOTIVATION OF RAN-AGNOSTIC COMMUNICATIONS

This section presents a simple but intuitive example showing that RAN-agnostic rate adaptation based on blind interference identification yields more reliable coexistence performance than the conventional SINR-based rate adaptation. In principle, when SINR decreases due to the interference from an incompatible RAN, SINR-based rate adaptation updates its

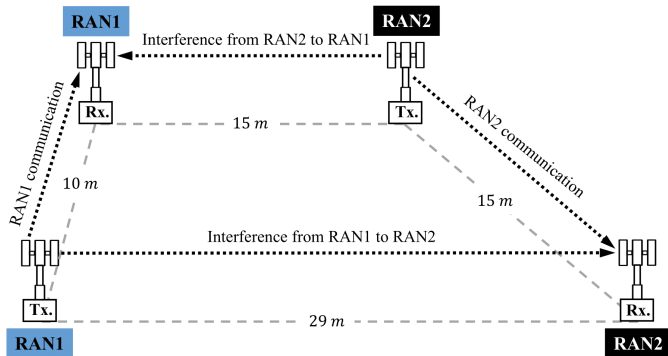


Fig. 1. RAN1-RAN2 coexistence scenario

modulation to a less susceptible one to the interference, e.g., adapting from QPSK to BPSK. On the contrary, identifying specific features of interference allows the RAN-agnostic rate adaptation method to select a more optimized modulation scheme leading to higher throughput and reliability, e.g. adjusting from QPSK to phase- and power-tuned QPSK.

Our toy example considers two incompatible RANs, RAN1 and RAN2, each with a transmitter-receiver (TR) pair, as illustrated in Fig. 1. We assume RAN1 is capable of RAN-agnostic rate adaptation while RAN2 follows SINR-based rate adaptation. For RAN1, the distance between its transmitter and receiver (henceforth mentioned as ‘TR distance’) is 10 meters, while the TR distance of RAN2 is 15 meters. In addition, the transmitter of RAN2 is 15 meters away from the receiver of RAN1, and the transmitter of RAN1 is 29 meters away from the receiver of RAN2. We also assume each transceiver pair performs single-carrier transmission via a 20 MHz channel with the carrier frequency of 2.4 GHz, while the transmit power is initially set to 100 mW. Each channel is assumed to follow a simple path-loss model, such as

$$\text{path-loss} = 10\gamma \log_{10}(4\pi d/\lambda), \quad (1)$$

where $\gamma = 2$ is the path-loss exponent, d is the TR distance, and λ is the wavelength.

If the two RANs do not coexist, RAN1 would use QPSK while RAN2 would select BPSK, both based on the measured signal-to-noise ratio (SNR) at each RAN’s receiver.¹ However, when they coexist as in Fig. 1, the BPSK signal from RAN2’s transmitter starts to interfere with RAN1’s receiver, making the receiver’s SINR significantly dropped from 8 dB to 2.2 dB. In case RAN1 adopts conventional rate adaptation, it would have no choice but downgrading its modulation to BPSK, risking reduced throughput.² The IQ-diagram in Fig. 2(a) shows the received symbol constellations of RAN1 contaminated by RAN2, where differently-colored four QPSK symbols are shifted in two directions due to interfering BPSK, resulting

¹We referred to the MCS(Modulation and Coding Scheme) table of IEEE 802.11ac, while considering the channel model in Eq. (1).

²RAN2 may stay with BPSK even though its SINR drops from 4.5 dB to 2.1 dB due to the interference from RAN1’s transmitter.

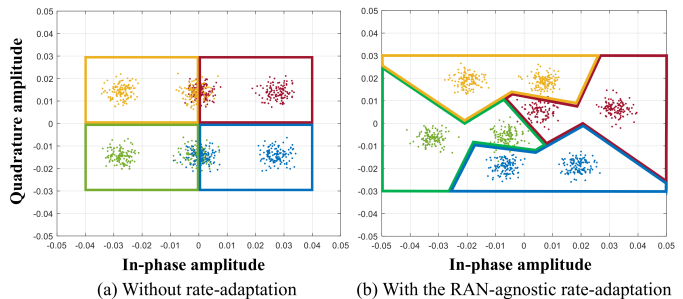


Fig. 2. The IQ-diagram of the received QPSK symbols for (a) plain QPSK and (b) QPSK with phase optimization

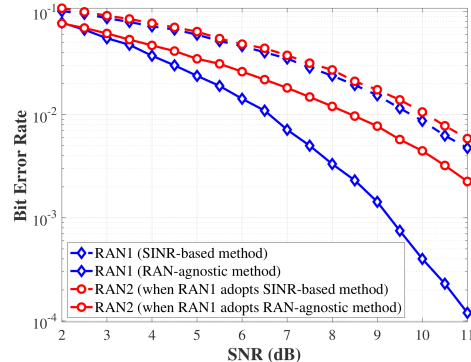


Fig. 3. BER curves of two rate-adaptation methods

in an overlapped constellation thus leading to degraded demodulation performance.

With blind identification of interference signal’s modulation type, however, RAN1 can further enhance the coexistence performance by preserving its QPSK but with optimized phase rotation. To show the effect, suppose RAN1 recognizes RAN2’s modulation type (i.e., BPSK) and runs RAN-agnostic rate adaptation to tune the plain QPSK to a modified QPSK with a phase rotation by $-\pi/6$, resulting in Fig. 2(b). As seen, the new IQ-diagram permits successful demodulation of contaminated QPSK symbols via structured symbol-by-symbol clustering. Fig. 3 presents the bit-error-rate (BER) curves of the two rate adaptation methods, which clearly shows that the RAN-agnostic method achieves a significant performance gain against the conventional one.

In general, the RAN-agnostic mechanism can evolve to optimize various communication parameters including modulation type, transmit power, phase rotation, etc. Nevertheless, this paper focuses on blind modulation identification, since it is the most fundamental building block of the RAN-agnostic communication technology while not fully investigated yet. Note that we reserve the problem of RAN-agnostic communication parameter optimization as our future work.

IV. RiSi: PROPOSED NEURAL NETWORK MODEL

This section first introduces backgrounds of semantic segmentation, and then elaborates RiSi, our proposed neural network for blind modulation identification of OFDMA signals.

A. Semantic Segmentation: Background

Semantic segmentation is a process of clustering the pixels of an image that belong to the same class. Unlike image classification where the label is assigned to an entire image, semantic segmentation's goal is to label each pixel with its corresponding class. Deep semantic segmentation is usually built on top of an image classification network, which serves as an encoder to obtain the local features of an image. Then, a decoder upscales those features back to the original image's size, and feeds them to the softmax layer where classification predictions are made.

A common architecture used for semantic segmentation is the fully convolutional network, which is achieved by replacing fully-connected layers with convolutional layers. Doing so significantly decreases the computational cost of training, as well as removes the input image size constraint allowing the network to be easily applied to variable-size images. A commonly used loss function in semantic segmentation, which is adopted in this paper, is the cross-entropy loss defined as:

$$L_{CE} = - \sum y \ln(t), \quad (2)$$

where y is the binary ground truth, t is the softmax layer output, and the summation is along all the pixels and classes.

B. Proposed Architecture of RiSi

The baseline of our proposed neural network is DeepLab V3+, a state-of-the-art fully convolutional neural network designed for semantic segmentation. Although vanilla DeepLab V3+ shows decent performance in vision processing, it was not instantly suitable for the wireless communications domain. Therefore, we propose its evolved version RiSi, by applying the expert knowledge in communications. Specifically, we replace its large two-dimensional convolutional filters with flattened convolutions [16], and also introduce the third image channel to have signal amplitude as an additional information.

The concept of flattened convolution comes from filter separation. The operation of convolution between image I and a convolutional layer with weights W is represented as:

$$I * W = \sum_{x'} \sum_{y'} \sum_c I(c, x - x', y - y') W(c, x', y'), \quad (3)$$

which is a function of x and y . Then, the flattened convolution tries to separate it into a series of 1-dimensional filters:

$$I * W = \sum_{x'} \left(\sum_{y'} \left(\sum_c I(c, x - x', y - y') \alpha(c) \right) \beta(y') \right) \gamma(x'), \quad (4)$$

where α , β , γ are the 1-dimensional filters. This paper only assumes spatial orthogonality, so we separate our filters as:

$$I * W = \sum_c \left(\sum_{x'} \left(\sum_{y'} I(c, x - x', y - y') \beta(c, y') \right) \gamma(c, x') \right). \quad (5)$$

Note that in the above, x and y represent two-dimensional coordinate of the image, and c implies the channel dimension.

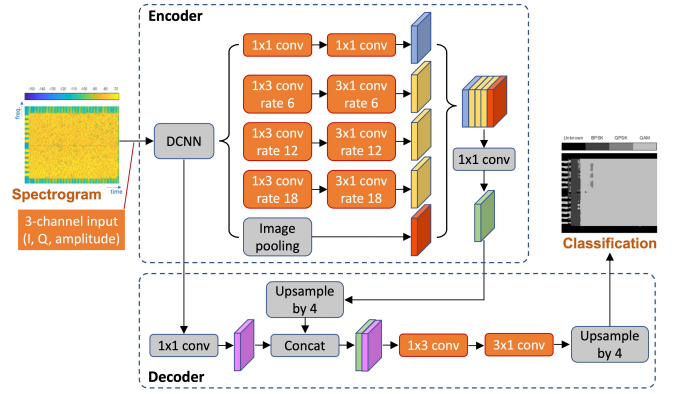


Fig. 4. Architectural diagram of RiSi (parts in orange are proposed revision)

The advantage of adopting flattened convolutions is three-fold. First, 1-dimensional filters have fewer parameters to optimize, thus speeding up the network training process. Second, due to the orthogonal nature between time and frequency, spectrograms would have lower ranks than usual images, making the flattened convolution a natural choice in the encoder layers. Third, since resource blocks have rectangular shapes by nature, we expect the segmentation output to be also rectangular. Since rectangular patterns have low ranks, such a grid-like pattern can be achieved by flattened convolutions in the decoder layers.

In addition to the adoption of flattened convolutions, we also attempt to use the third image channel (the blue channel of the RGB system, more specifically) that stores the signal amplitude as an additional information, to increase diversity in the input data. Note that we ruled out assigning the phase information to the third channel, due to its bounded and cyclic nature – when the phase is defined in the interval of $[-\pi, \pi]$, there would be discontinuity when calculating the gradient near the two bounds because the phase becomes identical after rotating a multiple of 2π .

Fig. 4 illustrates the architectural diagram of RiSi, where the orange-colored parts represent our proposal on how to revise the vanilla model.

C. Domain-specific Dataset Construction for RiSi

To achieve best-performing RiSi, it is also important to carefully generate the training dataset according to the intrinsic features of wireless signals using communications-specific knowledge, as introduced in the following. First, we built the dataset consisting of both synthetic samples and over-the-air recordings (of real WLAN signals captured by USRP N210 radios), to ensure that our model can perform well under real channel conditions. To make the synthetic dataset as close to real signals as possible, we modeled multiple channel defects to be employed in our system, such as fading, thermal noise, fractional frequency offset, and clock offset.³ Then, a random

³Specifically, we have employed the TGn channel delay model-B from the Matlab WLAN Toolbox, a white Gaussian noise with the SNR of 15 dB, a frequency offset uniformly distributed in $(-312.5, 312.5)$ kHz, and a clock offset uniformly distributed in $(-0.005, 0.005)$.

sequence of bits is OFDMA-modulated with the FFT(Fast Fourier Transform) size of 64, where each OFDMA resource block has a rectangular shape with a randomly-chosen size, and can take a modulation type out of BPSK, QPSK, 16-QAM, 64-QAM, unless it contains no data at all. We also consider the ‘no data’ class to address special situations communication protocols may encounter, e.g., when there exists no data indeed (such as ‘DC null’ in WLAN), or when a frame includes some fields modulated by non-popular specific schemes (such as header fields).

Practical OFDMA signals may include structures other than resource blocks, such us preambles, header fields, null, guard subcarriers, etc. While these structures have different sizes than OFDMA resource blocks, they still occupy rectangular regions in the spectrogram. We therefore want to make our system capable of detecting rectangular regions with varying sizes on a given spectrogram. To do so, in our synthetic dataset we varied the resource block size between data samples, so that RiSi is trained to detect the structures of different sizes, whose efficacy will be shown in Section V.

Thus-synthesized signals are used to obtain STFT(Short-time Fourier transform) based spectrograms with an FFT size of 256, the window length of 256, and the window shift of 8. The spectrograms are then transformed into 256x300 RGB PNG images, with the real and complex parts corresponding to the red channel and the green channel respectively. In addition, we also performed an experiment on the effect of using the blue channel to store the amplitude information of the signal, which will be also shown in Section V-B. Note that STFT is obtained by sliding a window function over the signal and applying DFT(Discrete Fourier Transform) to the windowed samples. More specifically, the STFT matrix of a signal $x(n)$ is defined as:

$$STFT_x(f, m) = \sum_{n=mK+1}^{mK+J} x(n)w(n - mK)e^{-j(\frac{2\pi f}{L})(n-mK)}, \quad (6)$$

where L is the FFT length, $w(n)$ is a window function, J is the window function length, and K is the window shift, while a rectangular window is adopted since it will produce the results closest to the OFDM demodulation.

Once we have generated signals as above, we should also consider how to organize the dataset in two aspects: how many samples to generate, and how much portion for each modulation type? We found that most related works utilized ‘tens of thousands’ to ‘hundreds of thousands’ of signal samples for training, with each sample containing dozens of symbols of a certain modulation type. In case of our experiment, each spectrogram sample contains thousands of data symbols of any modulation type, and hence we initially assumed that 10k (i.e., ten thousand) samples should be enough. Specifically, we generated 10k samples with four modulation types, BPSK, QPSK, 16-QAM, 64-QAM, which are evenly distributed in the dataset (i.e., each type is encountered with the same chance).

However, we discovered training on a dataset with 10k samples exhibits signs of overfitting in the early stages of

training. Moreover, thus-trained network not only showed poor performance but also had a trouble classifying between two QAM classes (see Fig. 6(a) in Section V). Intuitively, it makes sense that 16-QAM and 64-QAM would require more data samples due to their complex signal constellations compared to PSKs. Therefore, we appended 20k, 40k, and 90k additional samples consisting only of 16-QAM and 64-QAM data (with equal chance of appearance) to the original 10k samples, resulting in a total of 30k, 50k, and 100k samples respectively. The test results obtained with varying dataset sizes (i.e., 30k, 50k, 100k) have revealed that overfitting gets much mitigated and QAMs are more accurately classified as the dataset size increases, as will be shown in Section V-C.

V. IDENTIFICATION PERFORMANCE OF RiSi

In this section, we present a series of ablation studies based on extensive experiments, to analyze 1) the impact of replacing 2D convolutions with flattened convolutions, 2) the effect of introducing the third channel for the amplitude information of I/Q samples, along with two other channels representing I and Q samples respectively, and 3) the influence of dataset size and its organization on the modulation identification performance. Next, we evaluate the real-world performance of RiSi with the captured over-the-air WLAN packets. Finally, we compare RiSi’s performance with three existing networks in the literature, to show RiSi’s efficacy in OFDMA identification.

In the sequel, we have allocated 95%, 4%, and 1% of the dataset for training, validation, and testing, respectively, and we have used the initial learning rate of 0.001 and the learning rate drop of 0.8 every epoch. In addition, we have used the ADAM optimizer in each experiment, since we compared the performance of SGDM, RMSProp, and ADAM optimizers and concluded that ADAM gives the best performance. Note that all the training has been conducted by using Matlab Deep Learning Toolbox on NVIDIA GeForce RTX 3060 Ti.

A. Effect of Flattened Convolutions

Using flattened convolution in the decoder will serve as a ‘rectangularity’ constraint, since it will effectively require the output features to have lower ranks. To show its effect, we trained a network on a dataset of 10k samples, replacing conventional convolutions with flattened convolutions. Compared to the vanilla DeepLab V3+ (showing 77% accuracy), the proposed flattened network reaches 78.8% validation accuracy, achieving 1.8% enhancement. Note that we have used a two-channel version of RiSi to compare with the vanilla network (which is also two-channel based) for fairness.

It is also important to visually examine the effect of flattened convolutions to make sure they truly achieve a more rectangular output. Fig. 5 shows the segmentation outputs of the two networks, where we can see that the flattened network provides noticeably more rectangular shapes. Hence, our idea of using flattened convolution layers is proven to be effective in controlling the shape of the segmentation output as well as enhancing the performance.

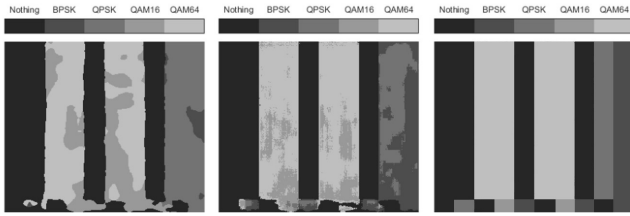


Fig. 5. Segmentation results comparison: vanilla DeepLab V3+ with 2D convolutions (left), our proposal with 1D convolutions (center), the ground truth (right)

B. 2-Channel vs. 3-Channel

In RiSi, we adopted three-channel input to increase diversity in the input data. To reveal its effect, we used the same signal set to generate the three-channel dataset and the two-channel dataset, and compared their resulting performances. In particular, we employed the three-channel version of RiSi (which is our proposal) and trained it on the three-channel dataset consisting of 10k samples. Then, the best validation accuracy we obtained was 79.8%, which is another 1% improvement from 78.8% reported in Section V-A. Therefore, adding an additional input data channel indeed has a beneficial effect on the performance.

C. Impact of Dataset Size

Section IV-C introduced our proposed strategy of constructing the training dataset considering different characteristics among modulation types. To show the efficacy of the strategy, we varied among 20k, 40k, 90k extra samples (consisting only of 16-QAM and 64-QAM) to be appended to the 10k samples (consisting of all four modulation types) and observed if the performance of the classifier can be improved with the additional data. Indeed, QAM classification accuracy turns out to much be risen from around 60% with 10k samples to 75% with 100k samples (see Fig. 6), with a slight decrease in PSK’s accuracy. The overall system accuracy with the 100k case reaches 86%, which is 6.2% enhancement from the 10k case. Further increase in the dataset size, however, did not show any significant enhancement in the classification accuracy.

From these results, we conclude that when creating datasets for modulation classification, the proportion of data samples per modulation scheme should be proportional to modulation complexity.

D. Performance with Real-captured Packets

To ensure the generalizability of our model to real world signals, we visually tested RiSi with the spectrograms of captured over-the-air WLAN packets. Fig. 7 shows multiple examples of RiSi’s performance with various captured WLAN packets. Then, Fig. 7(a) presents a BPSK beacon packet, and from the segmentation result we can clearly see the packet preambles and the header at the beginning, as well as a thin line of the DC null subcarrier. In addition, Fig. 7(c) shows a high-throughput 16-QAM data packet, from which we observe the BPSK header and the 16-QAM payload. Unfortunately, in

True Class \ Predicted Class	Nothing	BPSK	QPSK	QAM16	QAM64
Nothing	98.0%	0.4%	0.3%	0.3%	1.0%
BPSK	0.7%	93.4%	3.1%	1.0%	1.7%
QPSK	0.7%	2.0%	91.7%	3.8%	1.8%
QAM16	0.8%	1.8%	2.2%	64.0%	31.2%
QAM64	0.6%	1.0%	1.6%	38.0%	58.8%

(a) 10k dataset

True Class \ Predicted Class	Nothing	BPSK	QPSK	QAM16	QAM64
Nothing	97.3%	0.5%	0.8%	1.1%	0.3%
BPSK	0.6%	92.0%	4.1%	3.1%	0.2%
QPSK	0.4%	1.5%	93.6%	4.4%	0.1%
QAM16	0.8%	1.5%	4.1%	69.5%	24.1%
QAM64	0.4%	0.6%	2.0%	34.3%	62.7%

(b) 30k dataset

True Class \ Predicted Class	Nothing	BPSK	QPSK	QAM16	QAM64
Nothing	97.4%	0.0%	0.0%	0.4%	2.2%
BPSK	0.0%	91.0%	1.7%	4.6%	2.8%
QPSK	0.0%	1.2%	83.6%	12.7%	2.6%
QAM16	0.0%	0.1%	0.2%	67.9%	31.8%
QAM64	0.0%	0.1%	0.1%	30.1%	69.7%

(c) 50k dataset

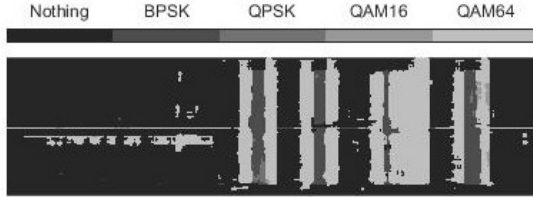
True Class \ Predicted Class	Nothing	BPSK	QPSK	QAM16	QAM64
Nothing	98.4%	0.0%	0.0%	0.3%	1.2%
BPSK	0.0%	92.9%	1.9%	3.2%	2.0%
QPSK	0.1%	2.2%	88.6%	7.3%	2.0%
QAM16	0.0%	0.1%	0.1%	75.0%	24.7%
QAM64	0.0%	0.1%	0.1%	24.4%	75.5%

(d) 100k dataset

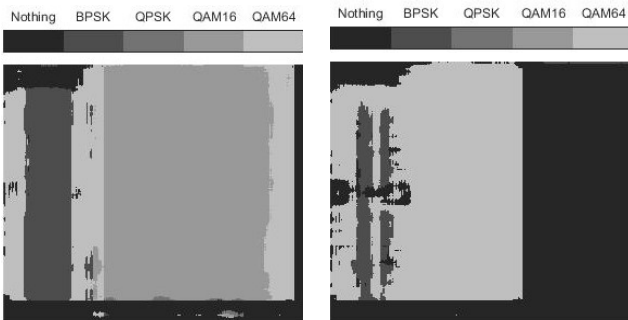
Fig. 6. Confusion matrices of RiSi trained on datasets with various sizes ('Nothing' means the 'no data' class)



(a) A WLAN beacon packet



(b) A burst of short frames



(c) 16-QAM data packet

(d) 64-QAM data packet

Fig. 7. A few examples of RiSi’s performance with real-captured WLAN packets (vertical axis: frequency, horizontal axis: time)

the presented cases, STF (the short training field in WLAN’s OFDM PLCP preamble) was mis-classified as 64-QAM, which makes some sense since STF has large amplitude variations between subcarriers making it looking like 64-QAM.

As a conclusion, we observed that our proposed network also works well with real-world signals and can be effectively utilized to visualize the structure of unknown data packets.

E. Performance comparison with other existing networks

To better judge RiSi’s contributions, we compared its performance with two other models taken from existing alternatives: the classifier proposed in [14] and Yolo in [17]. In the ‘simple classifier network’ in [14], the authors assigned ground truth classes as the most frequent modulation present in the spectrogram, and the accuracy is evaluated as mean pixel accuracy. On the other hand, a detector network with Yolo in [17] considered each resource block as an object to be detected. All the models (including RiSi) were trained on the same dataset with 10k samples, while RiSi is trained with the three-channel data and others are trained on the two-channel data. Note that we have used 10k samples to solely focus on the impact of RiSi’s architectural contributions (i.e., adopting flattened convolutions and three-channel inputs) against other methods.

	classifier in [14]	Yolo	RiSi (proposed)
overall	21.2%	16.5%	79.8%
no data	100%	66.0%	98.0%
BPSK	0%	4.0%	93.4%
QPSK	0%	3.0%	91.7%
16-QAM	0%	2.0%	64.0%
64-QAM	0%	6.0%	58.8%

TABLE I
IDENTIFICATION ACCURACY COMPARISON

The comparison result is summarized in Table I. As can be seen, the classifier in [14] and Yolo present a very poor accuracy in identifying the modulation types, which is in fact expected considering how they work. First, the classifier model can only correctly guess one of many modulations that may be present in the signal. That is, it treats the whole spectrogram as a single type of modulation, thus resulting in the ‘no data’ class. Next, although Yolo naturally identifies rectangular-shaped resource blocks via bounding boxes, its training process is severely hindered by a huge number of closely-packed resource blocks. This clearly signifies the necessity and efficacy of applying semantic segmentation to the blind identification problem of OFDMA signals.⁴

F. Discussion on the practicality of RiSi

For the aforementioned tests, we have also measured the inference time by RiSi to judge its practicality to be used in real systems, which is observed as around 2 milliseconds. Although it is not perfectly real-time, we claim that it is quite acceptable for serving RiSi’s fundamental goal, i.e., achieving better inter-RAN coexistence, because channels vary in the order of dozens of milliseconds in many practical scenarios [18]. That is, once a node equipped with RiSi recognizes the modulation type of a newly-appeared incompatible signal within 2 milliseconds, the node can adapt its modulation to better coexist with the signal for the remainder of time during which the channels of both parties do not change much (e.g., for a few dozens of milliseconds).

On the other hand, the training time has been measured as 2.5 hours for 10k samples and 20 hours for 100k samples, which suggests that the training time would be roughly proportional to the dataset size. Note that the observed training times are also acceptable since the training phase can be done offline in advance so that the trained RiSi can be deployed to each node.

VI. DOMAIN GENERALIZATION PERFORMANCE OF RiSi

Typically, a communication system is involved with numerous parameters (e.g., FFT size, CP length, etc.), but nevertheless we would like our proposed network to perform well under various communication environments. However, it is practically infeasible to fulfill the wish by simply employing a larger dataset with more diverse parametric variations, since a manageable-sized dataset cannot fully represent all possible combinations of parameter values. Moreover, as it will be

⁴It should be noted that RiSi’s fundamental performance is 86%, not 79.8%, which is achieved by our proposed dataset construction scheme in Section V-C.

shown in VI-B, even slight modifications to system parameters can significantly alter the appearance of the resulting spectrogram, thus deteriorating the network performance.

Therefore, it is necessary to study the ability of our network to extrapolate the signals unseen at the training stage. To do so, we utilize the same modulation classes that need to be recognized across the spectrograms of varying system parameters. Accordingly, we can address the issue of network generalization as a domain generalization problem by treating system parameters such as OFDM FFT size as different image domains.

A. Domain Generalization Techniques

In the AI community it has been known that machine learning algorithms suffer a significant performance loss when the test domain lies outside of the training distribution [19]. To address the problem, many domain generalization approaches have been proposed including MLDG(Meta-Learning Domain Generalization), a meta-learning based iterative approach to domain generalization. However in [20], the authors showed that simply using classical ERM(Empirical Risk Minimization) with accurate augmentation and hyperparameter optimization can outperform them all. In the mean time, a domain generalization method called SWAD(Stochastic Weight Averaging Densely) has been recently proposed [21], which argues that finding the region of a flat minimum improves the network’s generalization capabilities, showing 2% out-of-distribution improvement over existing approaches. Below are more details on ERM, MLDG, and SWAD.

- ERM is not a domain generalization method, but a general machine learning principle. In ERM, we assume that the test domain is unknown, so instead the model is trained to optimize its performance on training data. This is achieved via simple total loss minimization.
- MLDG [22] is a domain generalization method derived from MAML [23]. MLDG works by splitting the domains in the training set into meta-training and meta-validation domains at each iteration. After training on a batch of meta-train domain samples the network is then validated on meta-validation domains. The final update gradient of the network is determined by the weighted sum of the losses on meta-train and meta-validation data. Thus, the network is encouraged to learn the meta-train domains, while meta-validation ensures that the learnt features will improve the generalization capabilities.
- SWAD is an ensemble-based approach proposed in [21], which is an extension of SWA(Stochastic Weight Averaging) [24] to domain generalization. SWAD achieves generalization by averaging a series of weights obtained throughout conventional training of the network. It was proved in [24] that such averaging would result in a model that achieves the flat minimum, thus making it more robust to changes caused by a domain shift.

We hereby choose to compare the performance of ERM, MLDG, and SWAD, since we believe they can best represent a wide variety of domain generalization methods. It must be

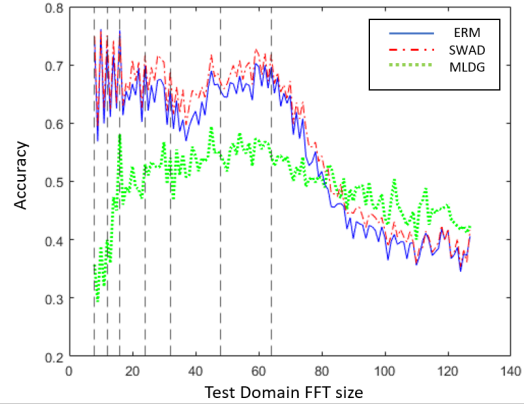


Fig. 8. Generalization performance comparison of various models on varying CP length domains. The vertical dashed lines imply the domains consisting of the training set.

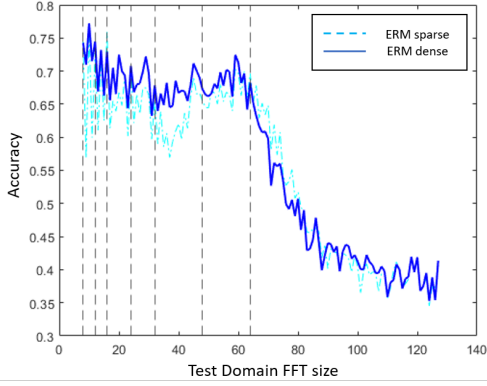
noted that ERM and SWAD have an advantage against MLDG thanks to their simplicity which allows them to be used without defining domains explicitly. On the contrary, MLDG may have problems due to the large number of potential domains that can be defined over the communication system and the way those domains may relate or interact with each other.

B. Domain Generalization Performance

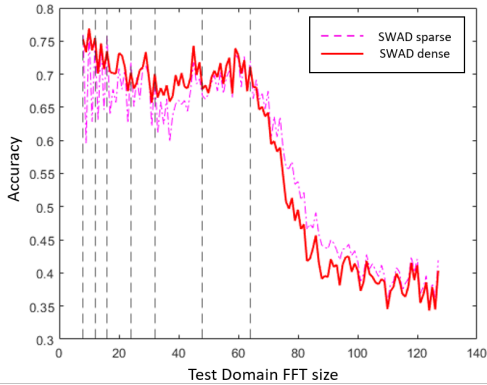
Until now, we have only considered OFDM signals with an FFT size of 64 and a cyclic prefix length of 8. For practical RAN-agnostic communications, however, we need to make our network to work satisfactorily with various signal parameters which may not be known in advance. Among such variations, we will treat varying FFT sizes or varying CP lengths as different domains, since the signals with the same modulation class could have completely different spectrograms if subcarrier spacing or the cyclic prefix length is changed, suggesting that the chosen two factors have great impact on the domain-generalized performance.

We first assume a fixed cyclic prefix length of 8 to focus on different ‘FFT size’ domains, and only consider 10k training dataset due to the added computational complexity of the training for domain generalization. We also have an independent test dataset that contains signals of every FFT size in the range from 8 to 128. The maximum FFT size that can be used in the training set is limited to 64, making the test signals with larger FFT sizes out-of-domain test cases.

Then, we compare the performance of ERM, SWAD, MLDG, when trained on the domains with FFT sizes of 8, 12, 16, 24, 32, 48, and 64, while using an initial learning rate of 0.002 in all three models. In ERM, the learning rate is exponentially decaying with a factor of 0.92. In SWAD, the network is trained in the same way as ERM for 10 epochs and then trained with a constant learning rate of 0.001 while the tolerance rate is set to 1.1. We also train MLDG with one meta-test domain left out at each episode, and use oracle validation (i.e., validating on the test set and choosing a model with the best performance) since MLDG does not define a



(a) ERM: sparse vs. dense



(b) SWAD: sparse vs. dense

Fig. 9. Training on dense and sparse datasets for ERM and SWAD

stopping criterion. Fig. 8 shows the test set accuracy for the test domains, revealing that SWAD is performing always better than ERM while MLDG’s performance is not promising except for FFT sizes larger than 80.

To justify our choice of sampled domains (i.e., ‘sparse’) for training instead of using all available domains of 8, 9, . . . , 64 (i.e., ‘dense’), we trained ERM and SWAD for sparse and dense cases, respectively, as shown in Fig. 9. It can be seen that although dense training does achieve better accuracy than sparse training, the gap is smaller for SWAD and the sparse case performs better out-of-domain with FFT sizes larger than 64 in both SWAD and ERM. Moreover, SWAD trained on the sparse dataset is performing almost as good as densely-trained ERM in-domain and has a superior performance out-of-domain for FFT sizes larger than 64. We conjecture that such improvement in out-of-domain performance with sparse dataset is due to the network being overwhelmed with all the domains in the dense training set.

Now, we repeat the experiment but with the FFT size fixed to 32 while varying the CP length which serves as different domains. The training set will only have the signals with the CP length varying from 0 to 8, while the test set will have a full variety of CP lengths. The results of this experiment are shown on Fig. 10. As shown, although the effect of the

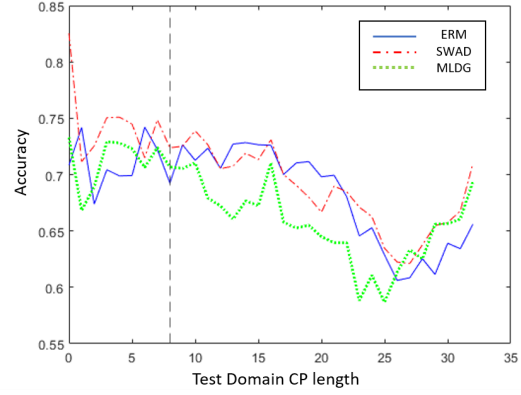


Fig. 10. Generalization performance comparison of various models on varying CP length domains. The domains in the lefthand side of the vertical dashed line are training domains.

Experiment	in-domain accuracy	out-of-domain accuracy
ERM (fixed CP)	62.2%	45.9%
SWAD (fixed CP)	67.8%	47.7%
MLDG (fixed CP)	51.2%	47.7%
ERM (fixed FFT)	70.9%	67.9%
SWAD (fixed FFT)	74.4%	68.6%
MLDG (fixed FFT)	71.2%	65.6%

TABLE II
SUMMARY OF EXPERIMENTAL RESULTS

CP length domain shift is not as substantial as that of FFT size, there is still an improvement after applying the domain generalization methods.

Table II summarizes the obtained mean accuracies for in-domain and out-of-domain performances, in two training scenarios: fixed CP length and varying FFT size, fixed FFT size and varying CP length. We can see that domain generalization methods, specifically SWAD, allow us to improve out-of-domain accuracy by approximately 1-2%, while also improving in-domain performance by 4-5%, all compared to ERM. We can also see that applying SWAD improves performance for both in-domain and out-of-domain cases. MLDG outperforms ERM in terms of out-of-domain accuracy in the fixed CP scenario, but the overall performance is poor. Overall, SWAD seems to be the best approach, consistently outperforming ERM by a few percents.

VII. CONCLUSION

This paper showed semantic segmentation can be successfully applied to the blind identification of OFDMA-modulated signals. Specifically, we proposed RiSi, a neural network architecture for blind modulation identification of OFDMA signals, fine-tuned from a state-of-the-art semantic segmentation mechanism. In addition, we verified the efficacy of the proposed architecture via extensive evaluations, and applied domain generalization techniques to our model to improve its performance with unseen system parameters, which showed that SWAD can achieve the best performance in dealing with unseen FFT sizes and CP lengths.

Considering the popularity of OFDMA in modern and upcoming wireless communication standards, we expect our work can be an important stepping stone in realizing truly RAN-agnostic inter-RAN coexistence in the near future. As a next step, we plan to extend the proposed work to be capable of differentiating and individually recognizing mixed interference signals. Based on such mechanisms, we will also investigate the issue of optimizing a set of transmission parameters of each RAN-agnostic RAN, to achieve better inter-RAN coexistence.

REFERENCES

- [1] 6G Flagship, “Key Drivers and Research Challenges for 6G Ubiquitous Wireless Intelligence,” University of Oulu, Tech. Rep., 2019.
- [2] K. David and H. Berndt, “6G Vision and Requirements: Is There Any Need for beyond 5G?” *IEEE Vehicular Technology Magazine*, vol. 13, no. 3, pp. 72–80, 2018.
- [3] D. Xia, J. Hart, and Q. Fu, “Evaluation of the Minstrel Rate Adaptation Algorithm in IEEE 802.11g WLANs,” in *Proc. IEEE ICC 2013*, 2013.
- [4] T. Araujo and R. Dinis, “On the Accuracy of the Gaussian Approximation for the Evaluation of Nonlinear Effects in OFDM Signals,” *IEEE Transactions on Communications*, vol. 60, no. 2, pp. 346–351, 2011.
- [5] L.-C. Chen et al., “Encoder-Decoder with Atrous Separable Convolution for Semantic Image Segmentation,” in *Proc. ECCV*, Sep. 2018.
- [6] N. E. West and T. O’Shea, “Deep Architectures for Modulation Recognition,” in *Proc. IEEE DySPAN*, Mar. 2017.
- [7] T. O’Shea and J. Hoydis, “An Introduction to Deep Learning for the Physical Layer,” *IEEE Transactions on Cognitive Communications and Networking*, vol. 3, no. 4, pp. 563–575, 2017.
- [8] T. J. O’Shea, T. Roy, and T. C. Clancy, “Over-the-air Deep Learning based Radio Signal Classification,” *IEEE Journal of Selected Topics in Signal Processing*, vol. 12, no. 1, pp. 168–179, 2018.
- [9] X. Liu, D. Yang, and A. El Gamal, “Deep Neural Network Architectures for Modulation Classification,” in *Proc. 51st Asilomar Conference on Signals, Systems, and Computers*, Oct. 2017.
- [10] X. Ma, D. Liu, and Y. Shan, “Intra-pulse Modulation Recognition using Short-time Ramanujan Fourier Transform Spectrogram,” *EURASIP Journal on Advances in Signal Processing*, vol. 2017, no. 1, 2017.
- [11] S. Jeong, U. Lee, and S. C. Kim, “Spectrogram-based Automatic Modulation Recognition using Convolutional Neural Network,” in *Proc. ICUFN*, Jul. 2018.
- [12] Q. Zhang, Z. Xu, and P. Zhang, “Modulation Recognition using Wavelet-assisted Convolutional Neural Network,” in *Proc. ATC*, Oct. 2018.
- [13] Y. Z. et al., “Spectrum Analysis and Convolutional Neural Network for Automatic Modulation Recognition,” *IEEE Wireless Communications Letters*, vol. 8, no. 3, pp. 929–932, 2019.
- [14] S. Jeong, U. Lee, and S. C. Kim, “Spectrogram-based Automatic Modulation Recognition using Convolutional Neural Network,” in *Proc. ICUFN*, Jul. 2018.
- [15] H. Changbo, H. Lijie, L. Guowei, and L. Yun, “Radar Signal Separation and Recognition based on Semantic Segmentation,” in *Proc. DSA*, 2020.
- [16] J. Jin, A. Dunder, and E. Culurciello, “Flattened Convolutional Neural Networks for Feedforward Acceleration,” in *Proc. ICLR*, May 2015.
- [17] A. Vagollari, V. Schram, W. Wicke, M. Hirschbeck, and W. Gerstaecker, “Joint Detection and Classification of RF Signals Using Deep Learning,” in *Proc. VTC2021-Spring*, Apr. 2021.
- [18] T. S. Rappaport, *Wireless Communications: Principles and Practice*, 2nd ed. Upper Saddle River, NJ, USA: Prentice Hall, 2002.
- [19] A. Torralba and A. A. Efros, “Unbiased Look at Dataset Bias,” in *Proc. CVPR*, Jun. 2011.
- [20] I. Gulrajani and D. Lopez-Paz, “In Search of Lost Domain Generalization,” in *Proc. ICLR*, May 2021.
- [21] J. C. et al., “SWAD: Domain Generalization by Seeking Flat Minima,” in *Proc. NeurIPS*, Dec. 2021.
- [22] D. Li, Y. Yang, Y.-Z. Song, and T. M. Hospedales, “Learning to Generalize: Meta-Learning for Domain Generalization,” in *Proc. AAAI*, Apr. 2018.
- [23] C. Finn, P. Abbeel, and S. Levine, “Model-Agnostic Meta-Learning for Fast Adaptation of Deep Networks,” in *Proc. ICML*, Aug. 2017.
- [24] P. I. et al., “Averaging Weights Leads to Wider Optima and Better Generalization,” in *Proc. UAI*, Aug. 2018.